


RESEARCH ARTICLE OPEN ACCESS

CCL2-CCR2 Axis Inhibition in Osteosarcoma Cell Model: The Impact of Oxygen Level on Cell Phenotype

Agne Petrosiute¹  | Justina Musvicaitė¹ | Donatas Petroška² | Alvilė Ščerbavičienė³ | Sascha Arnold¹ | Jurgita Matulienė¹ | Aurelija Žvirblienė⁴ | Daumantas Matulis¹ | Asta Lučiūnaitė⁴

¹Department of Biothermodynamics and Drug Design, Institute of Biotechnology, Life Sciences Center, Vilnius University, Vilnius, Lithuania | ²National Center of Pathology, Affiliate of Vilnius University Hospital Santaros Klinikos, Vilnius, Lithuania | ³Department of Biological Models, Institute of Biochemistry, Life Sciences Center, Vilnius University, Vilnius, Lithuania | ⁴Department of Immunology, Institute of Biotechnology, Life Sciences Center, Vilnius University, Vilnius, Lithuania

Correspondence: Agne Petrosiute (agne.petrosiute@gmc.vu.lt)

Received: 24 May 2024 | **Revised:** 14 October 2024 | **Accepted:** 6 November 2024

Funding: St. Baldrick's Foundation grant in part supported this study.

Keywords: CCL2 | CCR2 | osteosarcoma | tumor hypoxia

ABSTRACT

Treatment of osteosarcoma is hampered by tumor hypoxia and requires alternative approaches. Although the CCL2-CCR2 axis is indispensable in tumor-induced inflammation and angiogenesis, its blockade has not been effective to date. This study aimed to characterize how CCR2 inhibition affects the crosstalk of osteosarcoma cells with immune cells to better delineate tumor resistance mechanisms that help withstand such treatment. In this study, 143B cells were exposed to healthy donor PBMC supernatants in a transwell assay lacking direct cell-to-cell contact and subjected to different oxygen concentrations. In addition, mice bearing orthotopic 143B tumors were subjected to CCR2 antagonist treatment. Our findings show that hypoxic conditions alter cytokine and cancer-related protein expression on cells and impair CCR2 antagonist effects in the experimental osteosarcoma model. CCL2-CCR2 axis blockade in the 143B xenografts, which are positive for hypoxia marker CAIX, did not slow 143B tumor growth or metastasis but altered tumor microenvironment by VEGFR downregulation and shift in the CD44-positive cell population towards high CD44 expression. This study highlights differential responses of tumor cells to CCR2 antagonists in the presence of different oxygen saturations and expands our knowledge of compensatory mechanisms leading to CCL2-CCR2 treatment resistance.

Abbreviations: AFP, alpha fetoprotein; ANGPT1, angiopoietin 1; ANGPTL4, angiopoietin like-4; AP-1, activator protein 1; AREG, amphiregulin; ATX, lysophosphatidic acid; AXL, tyrosine-protein kinase receptor UFO; Bcl-x, B-cell lymphoma-x; CAIX, carbonic anhydrase isozyme IX; CAK1, mesothelin; CapG, macrophage-capping protein; CCL2, C-C motif chemokine ligand 2; CCR2, C-C motif chemokine receptor 2; CCL3, C-C motif chemokine ligand 3; CCL7, C-C motif chemokine ligand 7; CCL20, C-C motif chemokine ligand 20; CCL8, C-C motif chemokine ligand 8; CD, cluster of differentiation; CD25, interleukin-2 receptor alpha chain; CD66e, carcinoembryonic antigen-related cell adhesion molecule 5; CD105, endoglin; CD144, VE-cadherin; CD324, cadherin-1; CDKN1B, cyclin-dependent kinase inhibitor 1B; COL18A1, collagen alpha-1(XVIII) chain; CTSB, cathepsin B; CTSD, cathepsin D; CTSS, cathepsin S; CXCR1, C-X-C motif chemokine receptor 1; DCN, decorin; Dkk-1, dickkopf-1; DLL1, delta-1; ECM, extracellular matrix; ENO2, enolase-2; ENOS, nitric oxide synthase; ESR1, estrogen receptor alpha; FFPE, formalin-fixed paraffin-embedded; FGF2, fibroblast growth factor 2; FKH1, forkhead box protein O1 (FOXO1); FoxA2, forkhead box protein A2; FoxC2, forkhead box protein C2; GAL3, galectin-3; GM-CSF, granulocyte-macrophage colony-stimulating factor; gp40, epithelial cell adhesion molecule; H&E, hematoxylin and eosin stain; HER, epidermal growth factor receptor; HIF1A, hypoxia-inducible factor 1-alpha; HSP32, heme oxygenase; ICAM-1, intercellular adhesion molecule 1; IL, interleukin; IFN- γ , interferon gamma; IHC, immunohistochemistry; i.p., intraperitoneally; KLK, kallikrein; LECAM-2, endothelial-leukocyte adhesion molecule 1; LEP, leptin; LUM, lumican; M-CSF, macrophage colony-stimulating factor; MET, hepatocyte growth factor receptor; MSP, macrophage-stimulating protein; MFI, mean fluorescent intensity; MMP, matrix metalloproteinase; MUC, mucin; NKTS, natural killer T cells; OPN, osteopontin; p53, transformation-related protein 53; PDGF, platelet-derived growth factor; PBMC, peripheral blood mononuclear cells; PD-1, programmed cell death protein 1; PD-L1, programmed cell death ligand 1; PECAM1, Platelet endothelial cell adhesion molecule-1; PGN, progranulin; PRL, prolactin; ProgR/NR3C3, progesterone R; Serpin B5, maspin; Serpin E1, plasminogen activator inhibitor-1; SNAIL, zinc finger protein SNAIL; SPARC, osteonectin; Tie 2, angiopoietin receptor 2; TAM, tumor-associated macrophage; Tregs, T regulatory cells; TSP-1, thrombospondin 1; TME, tumor microenvironment; uPA, u-plasminogen activator; VCAM-1, vascular cell adhesion protein 1; VEGF, vascular endothelial growth factor; VEGFR, vascular endothelial growth factor receptor; VIM, vimentin.

This is an open access article under the terms of the [Creative Commons Attribution-NonCommercial-NoDerivs](https://creativecommons.org/licenses/by-nc-nd/4.0/) License, which permits use and distribution in any medium, provided the original work is properly cited, the use is non-commercial and no modifications or adaptations are made.

© 2024 The Author(s). *Journal of Cellular Physiology* published by Wiley Periodicals LLC.

1 | Introduction

Osteosarcoma, the most common bone cancer in children and young adults, continues to pose a treatment challenge. Survival of patients with localized disease is about 60%, and only 20% in patients with metastatic and recurrent tumors (Meltzer and Helman 2021). It has been recognized that the immune landscape in pediatric cancers differs from that of adults as pediatric cancers are primarily infiltrated by macrophages and lack T cell infiltration (Bosse et al. 2020; Thakur et al. 2022; Vakkila et al. 2006). This could be one of the reasons why novel immunotherapy strategies, such as immune checkpoint blockade, have failed to show efficacy in osteosarcoma (Meltzer and Helman 2021). In addition, tumor hypoxia negatively impacts any therapy (McDonald, Chafe, and Dedhar 2016). As tumors grow, they employ hypoxic microenvironment to their advantage via activating pro-inflammatory and proangiogenic pathways. Therefore, to improve osteosarcoma treatment outcomes, a better understanding of osteosarcoma biology is needed with a focus on macrophage/monocyte biology and hypoxia.

The CCL2-CCR2 axis is indispensable for cancer progression, as it is active in tumor hypoxia, neoangiogenesis, recruitment of immunosuppressing cells, and metastasis (Xu et al. 2021; Yoshimura 2018). Apart from cancer cells, CCR2 is also expressed in a plethora of cells such as monocytes/macrophages as well as T regulatory cells (Tregs), CD4⁺, CD8⁺ T cells, Natural Killer T cells (NKTs), endothelial cells, μ l and fibroblasts (Fei et al. 2021). Therefore, it serves as a crosstalk between cancer and immune cells. Although CCR2 can bind other ligands, such as CCL8, CCL12, and others, CCL2 has by far the highest binding affinity (Xu et al. 2021).

CCL2 considerably contributes to the recruitment of blood monocytes into the tumor microenvironment (TME) (Yoshimura 2018). This chemokine is also active during tumor hypoxia as hypoxic tumor-derived CCL2 drives the accumulation of granulocytic CD11b⁺/Ly6C^{med}/Ly6G⁺ myeloid cells in murine mammary tumors, which help to create the premetastatic niche. CCL2 neutralization in such a medium decreases metastatic tumor burden (Sceneay et al. 2012).

The CCL2-CCR2 axis is active in osteosarcoma patients and correlates with worse prognosis (Dou et al. 2021; Liu et al. 2020). Analysis of paraffin-embedded osteosarcoma specimens showed that all types of osteosarcoma had CCR2 gene expression (von Luettichau et al. 2008). Protein screening of patient samples showed significant CCL2 upregulation in tumor specimens compared to normal bone tissues (Dou et al. 2021). High-grade murine osteosarcoma cells produce more CCL2 than low-grade, while CCL2 knock-out cells decrease cell invasion (Chen et al. 2015). CCL2 is known as an enhancer of matrix metalloproteinase-9 (MMP-9) expression and cancer cell migration through CCR2 and activator protein-1 (AP-1) activation resulting in higher grade of the tumor (Liu et al. 2020). However, tumors have heterogeneous oxygen tensions. Tumor-related hypoxia significantly alters endothelial and immune cell landscape in TME and is one of the main causes of treatment resistance (Abou Khouzam et al. 2020). Therefore, it is crucial to examine CCL2-CCR2 axis changes in different oxygen environments and whether its inhibition in hypoxia differs from that in normoxia.

Here we aimed to study the differential effects of CCL2-CCR2 axis blockade in hypoxia compared to normoxia in the pre-clinical metastatic osteosarcoma human cell line 143B model (Uluçkan et al. 2015). We aimed to elucidate interaction mechanisms between osteosarcoma cells and immune cells in hypoxia versus normoxia and compensatory mechanisms involved when CCR2 is blocked. We used two approaches—an in vitro coculture of 143B cells with human peripheral blood mononuclear cells (PBMCs) and the in vivo mouse osteosarcoma xenograft model. We chose 143B cell and healthy donor PBMC coculture method as it better reflects in vivo cell behaviors and has emerged as an important method with various applications in cancer research (Oda et al. 2021; Rasouli and Safari 2024). Our coculture system is considered indirect as it lacks cell-to-cell contact and relies on communication via secretory factors (Rasouli and Safari 2024). To interrogate CCL2-CCR2 axis blockade we selected a small organic molecule RS504393 (spiropiperidine), a selective antagonist of the CCR2 receptor, that does not induce chemotaxis and does not stimulate post-receptor signaling (Mirzadegan et al. 2000). This compound blocks the CCR2 receptor by occupation of a binding site for CCL2 without affecting CXCR1, CCR1, or CCR3 (Mirzadegan et al. 2000). RS504393 has shown promising activity when used in combination with immune check blockade in solid tumor pre-clinical studies (Tu et al. 2020).

We interrogated the effect of the CCR2 antagonist on the ability of 143B cells to secrete chemokines CXCL8, CCL2, and vascular endothelial growth factor (VEGF). All these proangiogenic and pro-inflammatory chemokines play a role in osteosarcoma progression. In addition, we studied changes in the expression of various surface proteins on 143B cells that play a role in tumor hypoxia, such as carbonic anhydrase IX (CAIX), VEGFR, and programmed cell death ligand 1 (PD-L1). Moreover, we analyzed changes in CD44, a cell surface transmembrane glycoprotein crucial for the interaction between cancer cells and the extracellular matrix (ECM) and has been implicated in osteosarcoma progression (Mayr et al. 2017). Lastly, we performed proteome analysis for selected cancer-related targets on 143B cells in hypoxic and normoxic coculture with PBMCs with or without CCR2 antagonist treatment to assess changes in an array of cancer-related proteins.

Overall, our findings show how hypoxic conditions alter cytokine and receptor expression and impair CCR2 antagonist effect in the experimental 143B osteosarcoma model. We observed differential effects on protein surface expression, cytokine secretion and cancer-related protein makeup depending on oxygen levels. In the in vivo model, CCL2-CCR2 axis blockade with CCR2 antagonist did not slow tumor growth or metastasis but altered TME by VEGFR downregulation. Proteomics data from hypoxic coculture 143B cells show divergent protein expression patterns in response to CCR2 antagonist as compared to normoxia. These findings reinforce the role of hypoxia in CCL2-CCR2 axis inhibition failure.

Our data also reveals the potential use of a coculture model of tumor cells and PBMCs as a relevant model for studying cell phenotypes more accurately than mono-cultures.

2 | Materials and Methods

2.1 | Human Subjects

All healthy donor participants provided informed consent according to the declaration of Helsinki and the experimental protocols were approved by the bioethics protocol approved by the Vilnius Regional Committee of Biomedical Research (2020 03 31 #2020/3-1209-694, 2024 01 18 #2020/3-1209-694).

2.2 | Cell Culture

143B cells were purchased from ATCC. Cells were cultured in DMEM supplemented with 10% heat-inactivated fetal bovine serum and 100 units/mL penicillin, 100 mg/mL streptomycin. Cells were grown in the humidified incubator with 21% O₂, 5% CO₂ at 37°C. Hypoxic conditions, when needed, were achieved in the hypoxic chamber (MACS VA500 microaerophilic workstation, Don Whitley Scientific, UK) with 1% O₂, 5% CO₂, and residual N₂.

2.3 | Flow Cytometry (FC)

2.3.1 | FC on PBMCs and 143B Cells

Cells were stained with following anti-human antibodies: anti-h/mCD11b FITC (#101206, Biolegend), anti-hCD86 Alexa Fluor (AF) 488 (#53-0869-42, Invitrogen), anti-hCD274 APC (#17-5983-42, Invitrogen), anti-hCAIX AF488 (#FAB2188G, R&D), anti-hCD45 PE/Cy7 (#304016, Biolegend), anti-hVEGFR PE/Cy7 (#393008, Biolegend), anti-hCCR2 PE (#357206, Biolegend), anti-hCD206 APC (#17-2069-42, Invitrogen), anti-hCXCR1 FITC (#8F1-1-4, eBioscience). 7-AAD stain (#00-6993-50, eBioscience) was used to discern live cells from the dead. Cells were analyzed by flow cytometry using Partec CyFlow Space flow cytometer (Germany). For CXCR1 analysis cells were analyzed with BD FACS Symphony A1 cell analyzer (Becton, Dickinson and Company, USA). Data were analyzed using FlowJo. Cells were selected according to FSC-H and SSC-H plots. When duplicates were discriminated using FSC-H and FSC-A plots. 7-AAD negatives cells were used for the analysis.

2.3.2 | FC on Tumors, Harvested From Mice

Tumors were dissected from mice and placed into a separate 100 mm Petri dish on ice, quickly minced with scalpels into fragments. Collagenase 1 mg/mL and DNase (Roche #52779120) 100 µl/2 mL added into 2 mL HBSS and incubated at 37°C for 15 min. Digested tumors were passed through a 70 µm strainer. Cells were centrifuged, lysed with 2 mL ACK lysing buffer for 1 min to deplete red blood cells, quenched with HBSS, centrifuged and washed with FACS buffer, and subjected for flow analysis. TruStainFcX (#422302, Biolegend) was used for non-specific receptor blockade. To analyze tumor fraction in human cell xenografts anti-hCD274 APC (#17-5983-42, Invitrogen), anti-hCA9 AF488 (#FAB2188G, R&D), anti-hVEGFR PE/Cy7 (#393008, Biolegend), anti-hCCR2 PE (#357206, Biolegend), anti-hCD44 APC (#559942, BD Pharmingen) with corresponding

isotype controls. For immune fraction in xenograft tumors, anti-mouse antibodies were used. For nonspecific receptor blockade, TruStainFcX anti-mouse (#101320, Biolegend) was used. Antibodies used were anti-h/mCD11b FITC (#101206, Biolegend), anti-mCD206 APC (#141708, Biolegend), anti-mCD86 PE (#105008, Biolegend), anti-mPD-L1 PE (#155404, Biolegend), anti-mCCR2 PE (#150610, Biolegend). 7-AAD stain (#00-6993-50 eBioscience) was used to discern live cells from dead. Cells were analyzed by flow cytometry using BD FACS Symphony A1 flow cytometer (USA). Data were analyzed using FlowJo. Cells were selected according to FSC-A and SSC-A plots. When duplicates were discriminated using FSC-H and FSC-A plots. 7-AAD negatives cells were used for the analysis.

Fraction of positive cells (%) or mean fluorescent intensity (MFI) of certain marker were calculated and used for further analysis.

2.4 | Transwell 143B–PBMC Assay

For transwell assay Thermo Scientific, Nunc Polycarbonate Cell Culture Inserts in Multi-Well Plates, 0.4 µm, 12-well (#140652) were used. First, 0.15×10^6 143B cells per well were seeded and left for 24 h in 1% O₂ in Advanced DMEM with 3%FBS (#12491-015, Gibco). Treatment with vehicle or RS504393 (#2517, Torcris) 0.5 µM concentration was added and cells were incubated in 21% and 1% O₂. After 24 h, healthy donor blood was collected in compliance with the bioethics protocol approved by the Vilnius Regional Committee of Biomedical Research (2020 03 31 Nr.2020/3-1209-694). PBMCs were isolated using Ficoll-Paque PREMIUM (#17-5442-02, GE Healthcare) according to manufacturer protocol. Cells were counted and seeded 1×10^6 per well with Advanced DMEM + 5% BSA. After 48-h incubation in 1% or 21% O₂, supernatants were collected from the top or bottom chambers, centrifuged 300 × g for 5 min. Gathered supernatant was centrifuged again 1000 × g for 5 min, and prepared for ELISA analysis. PBMCs from the top chamber and 143B cells from the bottom chamber were harvested for flow analysis.

2.5 | Quantitation of Cytokines and Chemokines in Cell Culture Supernatants

Indirect enzyme-linked immunosorbent assay (ELISA) kits for the measurement of human cytokines and chemokines—CCL2, CXCL8 (#88-7399-88, #88-8086-86, Invitrogen, Thermo Fisher Scientific, USA), VEGF (#DY293B-05, R&D Systems) – levels in cell culture supernatants were used. ELISA kits are based on the sandwich immunoassay technique. Supernatants were used diluted up to 1:200. All procedures were performed according to manufacturers' protocols. In the last step 3,3',5,5'-tetramethylbenzidine (TMB) substrate solution was added to each well. The plates were monitored for 15 min for color development, the reaction in wells was stopped with 3.6% H₂SO₄ solution and the wells were read at 450 nm with reference wavelength at 620 nm using Multiscan GO microplate spectrophotometer. A standard curve was generated from cytokine standard and the cytokine concentration in the samples was calculated.

2.6 | 143B Xenograft Experiment

Female Nude mice (CR ATH HO Code 24106216), 5–6 weeks old, were obtained from Charles River Laboratories. Animals were housed, bred, and handled in the Department of Animal Models Animal Facility at Life Sciences Center, Vilnius University, Lithuania, 12-h light-dark cycle, at 21°C–23°C and 40%–60% humidity. Animals were fed with an irradiated breeding/maintenance diet for transgenic mice (Altromin, #1414) and water ad libitum. All experimental procedures conformed to Directive 2010/63/EU requirements and were approved by the Lithuanian State Food and Veterinary Service (Approval No. G2-233, 2023-01-18).

Before injection into animals, mycoplasma-free 143B cells in the exponential growth phase were harvested, washed, and re-suspended in PBS. 8–12 weeks old female Nude mice were inoculated intraosseous under isoflurane anesthesia with 0.5×10^6 143B cells resuspended in 20 μ L of PBS into the right tibia. Once tumors reached palpable size, on the 16th day post-tumor inoculation, mice were randomized based on tumor size and treated with CCR2 antagonist RS504393 (#2517, TOCRIS) at a dose of 2 mg/kg/dose intraperitoneally (i.p.) daily or vehicle control. 10 mice per group were used based on sample size calculation guidelines (Arifin and Wan Mohammad 2017). Tumor size was calculated as follows: volume = $(D \cdot d^2 \cdot \pi) / 6$, where D is the longer measurement and d is the shorter one. All mice were sacrificed once a single mouse reached a tumor volume of 1500 mm³. At the end of the experiment, animals were euthanized with a flow of 8.0 L/min of medical CO₂ gas (Elme Messer Lit, Vilnius, Lithuania) followed by cervical dislocation.

2.7 | Immunohistochemistry

Immunohistochemistry on 143B tumors and lungs was performed by the National Pathology Center, Vilnius, Lithuania. Formalin-fixed and paraffin embedded (FFPE) slides cut at 3 microns were subjected to H&E and immunohistochemical staining with BenchMark Ultra VENTANA. In brief, before initial deparaffinization, sections were steamed in 60°C for 24 min, then antigen retrieval with CC1 for 64 min at 95°C. The slides were incubated against CCR2 antibody (Roche clone SN707, 1:400; frozen at –20°C) for 32 min at 37°C and CAIX antibody (clone EP161, 1:50, #379R, cell marq). Tissues were exposed to Dab chromogen 8 min and then counterstained with hematoxylin, dehydrated, and mounted. Visualization system universal DAB detection kit (#(92) 760-500, Roche) was used. Metastasis count was analyzed by two investigators. Total metastasis burden per mouse was estimated by measuring their size and applying the following formula: volume = $(D \cdot d^2 \cdot \pi) / 6$, where D is the longer measurement and d is the shorter one.

2.8 | Proteome Profiler Analysis

Proteome analysis on 143B cells, harvested from mono-culture and coculture with healthy donor PBMCs, was performed using Proteome Profiler Human XL Oncology Array Kit (#ARY026,

R&D) following manufacturer's instructions. Briefly 143B cells lysates (one lysate from three donors per treatment condition) were prepared using RIPA lysis buffer (#89900, ThermoFisher) containing protease and phosphatase inhibitors (ThermoFisher Halt Phosphatase inhibitor cocktail (#78428) and Halt Protease Inhibitor Cocktail (#78425) and PMSF Protease Inhibitor (#36978)) for 30 min on ice and centrifuged at 16,000 \times g for 15 min at 4°C. Total protein lysate was quantified using the Bradford method. 400 μ g of lysate was used per condition. Images were obtained using the Alliance Q9 Advanced (UVITEC) system. Spots were quantified using the UVIBAND MAX analysis software system. Pixel density signal of each spot, representing one analyte, was quantified. Each analyte had two repeats, so an average value of each pair was used. Quantified average signal value of each spot was subtracted by an average background value (negative control in the array kit). In the case the subtracted signal value was equal 0 or lower, it was equalized to 1 for further analysis. Calculated values were used for multiple variable analysis (all calculated values are represented in Supporting Information Table S1, raw blots in Figure S1). Relative changes (log(fold change)) of calculated signal values were used for heatmaps to compare the change in protein expression level.

2.9 | Statistical Analysis

Statistical analysis was performed using GraphPad Prism (version 10.0.2). A parametric unpaired *t*-test was applied to evaluate the statistical significance of differences between two independent groups of variables and $p < 0.05$ was assumed to be significant (* $p < 0.05$; ** $p < 0.01$, *** $p < 0.001$, **** $p < 0.0001$).

3 | Results

3.1 | CCR2 Expression and CCL2 Secretion Are Increased in 143B Cells in the Presence of PBMCs

First, we determined the secretion level of CCL2 and CCR2 expression patterns in 143B cells. CCR2 expression on 143B cells is not robust in vitro, but it is more evident in vivo (Figure 1A). 143B cells secrete CCL2, more in normoxia than in hypoxia, but it can acutely increase by IFN γ stimulation (Figure 1B).

We assumed that the crosstalk of 143B cells with immune cells can provoke CCL2-CCR2 axis activation. Therefore, we assessed the changes in CCR2 and CCL2 on 143B cells when they were subjected to secretory factors from PBMCs by employing a healthy donor PBMC coculture model using the transwell assay. In such system, 143B cells were seeded on the bottom of the transwell vessel for 24 h either under normoxia and hypoxia conditions. The PBMCs were collected from healthy adult donors the next day, seeded on the 0.4 μ M pore size top chamber of the transwell, and incubated either under normoxia and hypoxia for an additional 48 h. In such a system, cell communication lacked direct cell-to-cell contact. Although CCR2 expression on 143B cells did not change, we discovered a significant increase in CCR2 expression on CD11b⁺ PBMCs in

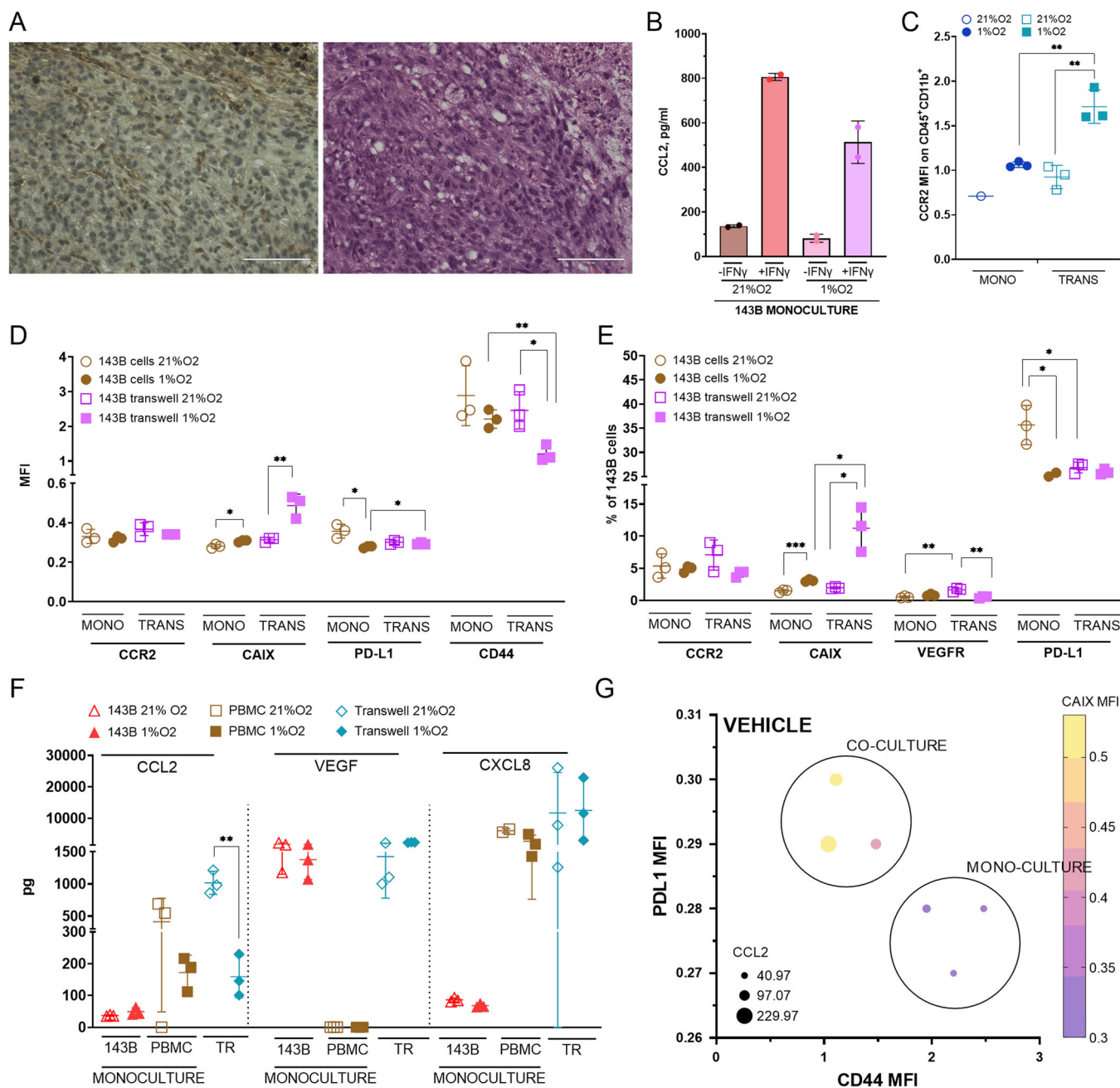


FIGURE 1 | 143B cell phenotype in mono-culture and coculture with immune cells. (A) CCR2 expression (left) and H&E stain (right) on 143B tumors by immunohistochemical analysis (IHC); scale bars=100 μ m. (B) ELISA analysis for differences in CCL2 secretion of 143B cells grown in normoxia or hypoxia, without/with (-/+ IFN γ). (C) CCR2 expression differences by MFI on CD11b cells when PBMC are grown in mono-culture (blue circles) and in transwell (teal squares) in normoxia (empty shapes) or hypoxia (filled shapes). (D) Changes of surface protein expression by mean fluorescent intensity (MFI) of the following markers: CCR2, CAIX, VEGFR, and PD-L1, when 143B cells were grown in mono-culture (brown circles), they were exposed to PBMC cells in a transwell assay (coculture, purple squares) under normoxia (empty shapes) or hypoxia (filled shapes). (E) Changes in percentage of surface protein expression of these markers: CCR2, CAIX, VEGFR, PD-L1, and CD44, when 143B cells are grown in mono-culture (brown circles) or when they are exposed to PBMC cells in a transwell assay (purple squares), either under normoxia (empty shapes) or hypoxia (filled shapes). (F) Secretion of CCL2, VEGF and CXCL8 by 143B cells (pink triangles) or PBMC (red squares) in mono-culture, in transwell (teal rhombi) under normoxia (empty shapes) or hypoxia (filled shapes). (G) Multiple variables analysis for PD-L1, CCL2, CD44 and CAIX expression in hypoxia comparing transwell coculture phenotype with mono-culture. * $p < 0.05$, ** $p < 0.01$, *** $p < 0.001$, significance was determined using the Student's t -test, $n = 3$ per experimental group.

hypoxia when compared to cell mono-culture and normoxia (Figure 1C), whereas CCR2 expression on tumor cells did not change significantly. CCL2 secretion was minimal by 143B cells under normoxia and hypoxia, but increased by PBMCs

(Figure 1F). CCL2 secretion increased in the transwell system under normoxia but decreased significantly in hypoxia (Figure 1F). Although we observed a decrease in CCR2 expression on 143B cells as well as CCL2 secretion by 143B cells

and PBMCs in hypoxia compared to normoxia, the surface expression of CCR2 on CD45⁺CD11b⁺ PBMCs increased in hypoxia.

3.2 | Hypoxia Causes Downregulation of CD44, VEGF, and PD-L1 and an Increase in CAIX Surface Expression in 143B Cells in the Coculture Model

Hypoxia increased CAIX expression in 143B cells and it was even more prominent in a transwell assay (Figure 1D,E). PD-L1 expression decreased in hypoxia and in transwell assay (Figure 1D,E). Similarly, CD44 expression decreased in hypoxia in cell mono-culture and transwell (Figure 1D). Although VEGFR expression increased in transwell in normoxia, it decreased in hypoxia (Figure 1E). We found that VEGF secretion was prominent by 143B cells, but not PBMCs (Figure 1F) as opposed to CXCL8 secretion, which was primarily secreted by PBMCs and increased when cells were grown in a transwell system, more so in hypoxia (Figure 1F).

To describe cell phenotype comparing mono- and co-cultures, we performed multiple variables analysis of surface protein expression changes in hypoxia. We found changes in total CCL2 secretion, and expression of PD-L1, CD44, and CAIX on 143B (Figure 1G) in the coculture compared to mono-culture of 143B cells.

3.3 | CCR2 Inhibition Causes a Different Pattern of Cell Response in the Co-Cultures and Mono-Cultures of 143B Cells and PBMCs under Normoxia and Hypoxia Conditions

To assess the change in tumor cell phenotype after CCR2 inhibition, we investigated the secretion levels of cancer-related chemokines and expression of cancer and immune cell activation markers on 143B cells and PBMCs grown either in mono-culture or coculture. CCR2 antagonist decreased CXCL8 secretion by PBMCs (more under normoxia conditions), but did not significantly alter its secretion in a transwell assay (Figure 2A). CCR2 antagonist decreased VEGF secretion in transwell under hypoxic conditions (Figure 2B), but not in 143B cells in mono-culture. CCR2 inhibition increased CCL2 secretion in PBMC mono-culture as well as transwell under both, hypoxia and normoxia (Figure 2C). Comparing surface protein expression on 143B cells in their coculture with PBMCs under normoxia and hypoxia conditions, we observed that CCR2 inhibition increased CD44 and PD-L1 expression on 143B cells only in normoxia and increased VEGFR in both, normoxia and hypoxia, conditions (Figure 2D,E). There was a notable trend of decreased CAIX expression in hypoxia after the addition of CCR2 antagonist (Figure 2D,E). We also analyzed CXCL8 receptors' CXCR1 and CXCR2 changes on 143B cells and PBMCs when they were grown as mono-culture or in coculture. We did not detect CXCR2 receptor expression either on 143B cells or on PBMCs (data not shown). At the same time, CXCR1 receptor expression on 143B cells in mono-culture increased significantly in hypoxia compared to normoxia (Figure 2F). Interestingly, CXCR1 expression increased similarly in normoxia when 143B cells were grown in transwell (Figure 2F). This can be explained by a prominent CXCL8 secretion by

PBMCs. CCR2 inhibition did not have significant effects on CXCR1 expression (Figure 2F).

Next, we summarized the CCR2 antagonist effects on cytokine secretion and surface protein expression in hypoxia using multiple variables analysis. By applying multiple variables analysis to cells treated with CCR2 antagonist in hypoxia, we noticed a change in cell phenotype described by a decrease in expression of PD-L1 and CD44, as well as an increase in CCL2 secretion and CAIX expression in the coculture as compared to mono-culture (Figure 2G). Lastly, comparing CCR2 antagonist effects on cells treated with vehicle-only in the coculture under hypoxia, we observed a decreased VEGF secretion and diminished expression of CD44 and CAIX on 143B cells, as well as an increased CCL2 secretion (Figure 2H). Overall, CCR2 inhibition effects were more pronounced in the coculture model than in the mono-culture.

Lastly, we determined changes in CD11b⁺CD86⁺, CD11b⁺CD163⁺, CD11b⁺CD206⁺, CCR2⁺, CD11b⁺CCR2⁺, and PD-L1⁺ percentage of CD45⁺ cells by flow cytometry on PBMCs that were cocultured with 143B⁺/– CCR2 antagonist under hypoxic or normoxic conditions. No significant changes were noted except for a CCR2⁺ increase on CD45 when a CCR2 antagonist was added in normoxia (Figure 2I) and it is likely a compensatory effect.

3.4 | In vivo Treatment With CCR2 Antagonist Does Not Affect Tumor Growth or Metastasis But Causes Phenotypic Changes in 143B Cells and Tumor-infiltrating Monocytes/Macrophages

To assess 143B tumor growth in vivo under CCR2 inhibition, 143B cells were inoculated intraosseous into the right tibia of Nude mice. Once tumors reached palpable size, we randomized them into two treatment groups ($n = 10$ per group). We started treating tumors with the CCR2 antagonist RS504393 at a dose of 2 mg/kg/dose i.p. daily on the day of randomization. Treatment did not induce differences in tumor growth (Figure 3A) or metastatic burden in lungs from mice who received CCR2 antagonist compared to vehicle control (Figure 3B,C). At the end of the experiment, tumors were harvested from mice and subjected to flow cytometry analysis. We analyzed surface protein expression on tumor cells and some immune cells, mainly murine monocytes/macrophages, since these xenografts were grown in Nude mice with impaired T cells. Interestingly, we observed two tumor cell populations having different expressions of CD44 (Figure 3D, CD44^{low} and CD44^{high}). The ratio of these populations changed after treatment with CCR2 antagonist. CCR2 inhibition equalized the percentages of cells in each population by increasing the number of CD44^{high} cells (Figure 3D,E). When analyzing tumor cell fraction by flow cytometry, we observed no changes in CCR2 or PD-L1 surface expression in tumor cells of mice who received CCR2 antagonists (Figure 3F). However, the VEGFR signal decreased statistically under CCR2 inhibition (Figure 3F). When surveying monocytes/macrophage cell population we observed increased infiltration of CD11b⁺CD86⁺ cells into the tumor (Figure 3G). However, we did not detect the change in a fraction of CD11b⁺CCR2⁺ cells (Figure 3G).

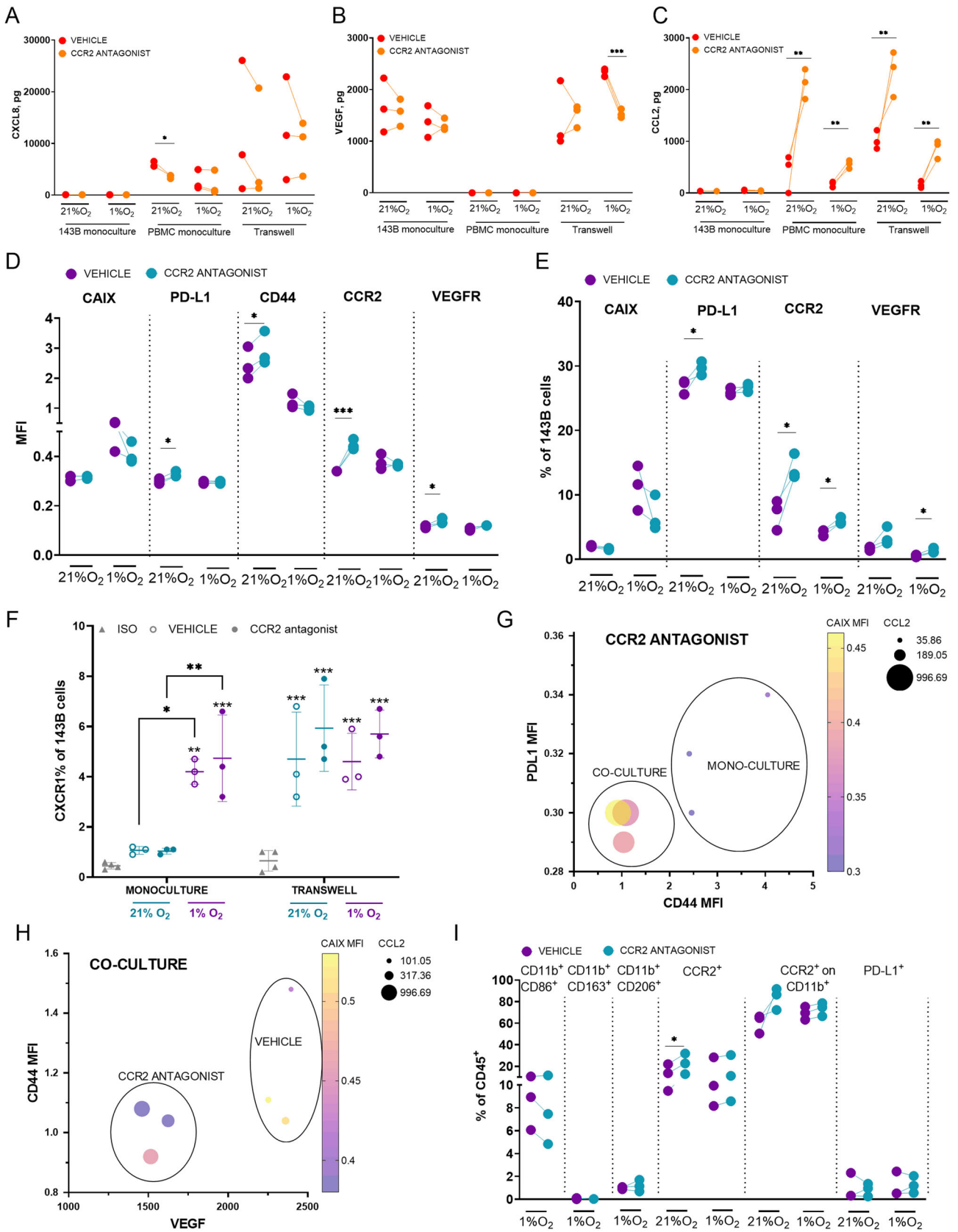


FIGURE 2 | Legend on next page.

Lack of response to CCR2 antagonist *in vivo* can be linked to tumor hypoxia. Hypoxia is a prominent feature in 143B tumors (Campanile et al. 2013). In agreement with that, 143B tumors from our experiment had pronounced expression of hypoxia-induced protein CAIX by flow and IHC (Figure 3H,I) (McDonald and Dedhar 2014).

3.5 | Proteome Analysis for Selected Cancer-Related Targets of 143B Cells Grown as Mono-Culture or in Coculture With or Without CCR2 Antagonist Treatment Reveals Global Upregulation of Cancer-Related Proteins in Cells From Coculture as Well as Differential Response to CCR2 Antagonist in Hypoxia Versus Normoxia

Lack of response to CCR2 antagonist treatment *in vivo* prompted us to go back to coculture experiments. We went on to analyze cancer-related protein changes in cocultured 143B cells in different oxygen environments when they are exposed to CCR2 antagonists versus vehicle controls. We performed a proteome array on these cells using the Human XL Oncology Array Kit. First, we assessed changes in 143B cells when they were harvested from transwell versus from mono-culture. We observed a global increase in the majority of tested cancer-related proteins in coculture (Figure 4A) highlighting the beneficial utility of the coculture model. More importantly, treatment with CCR2 antagonist of 143B cells in coculture revealed differential upregulation of various proteins in normoxia as compared to hypoxia (Figure 4B). We grouped these proteins in clusters based on function and observed that proteins that are involved in extracellular matrix remodeling, such as kallikrein 5 (KLK5), cathepsinB (CTSB) are decreased with CCR2 antagonist treatment in hypoxia, but upregulated in normoxia. In contrast, matrix metalloproteinase-3 (MMP-3) is upregulated by CCR2 antagonist in hypoxia but downregulated in normoxia (Figure 4B). Similarly divergent response was identified in the analysis of adhesion proteins (PECAM-1, LECAM-2, gp40, cadherin 1 (CD324) are decreased in response to CCR2 antagonist in hypoxia, but increased in normoxia. On the contrary, carcinoembryonic antigen-related cell adhesion molecule 5 (CD66e) and amphiregulin (AREG) are increased in response to CCR2 antagonist in normoxia, but not hypoxia (Figure 4B). Angiogenesis proteins are also affected differentially. Such as endoglin (CD105), angiopoietin 1 (ANGPT1), serpin E1, VEGF are decreased in response to CCR2 antagonist in hypoxia but are upregulated in normoxia, whereas cadherin-5 (CD144) and

thrombospondin1 (TSP-1) are increased in hypoxia, but decreased in normoxia (Figure 4B). Proteins that are associated with drug resistance, such as AXL are decreased in hypoxic coculture but increased in normoxic, when CCR2 antagonist is added, whereas delta-like ligand 1 (DLL1) and Serpin B5 show contrary trends. Immune signals such as interleukin-2 receptor alpha chain (CD25), granulocyte-macrophage colony-stimulating factor (GM-CSF), CXCL8, and CCL8 also show contrasting expressions in hypoxia versus normoxia (Figure 4B). Interestingly CCR2 antagonist upregulates HIF1A and CAIX expression in hypoxia, but decreases VEGF and angiopoietin-like 4 (ANGPTL4) expressions (Figure 4B). Overall, we found contrasting protein expression patterns in 143B cells in response to CCR2 antagonists under hypoxic and normoxic conditions.

To better delineate oxygen gradient-dependent differences in response to CCR2 antagonist on 143B cells in coculture we depicted multiple variables analysis for various cancer-related proteins in hypoxia versus normoxia comparing transwell coculture phenotype when cells are treated with vehicle versus CCR2 antagonist. We grouped 143B cells in clusters according to signaling pathways: adhesion (Figure 5A), immune signaling (Figure 5B), drug resistance (Figure 5C), angiogenesis (Figure 5D), hypoxia (Figure 5E), metabolic and tumor suppressing factors (Figure 5F). Again data shows divergent CCR2 antagonist response in hypoxia as compared to normoxia. Increase in HIF1A, CAIX, p53, MMP3, AREG, CD66e can be associated with treatment resistance and are targetable.

4 | Discussion

In this study, we attempted to elucidate CCL2-CCR2 axis-driven mechanisms of osteosarcoma tumor evasion in metastatic osteosarcoma cell line 143B model in different oxygen micro-environments. In addition, we evaluated the effects of pro-inflammatory and proangiogenic factors when CCR2 was inhibited. We assumed that for this approach cancer-immune crosstalk is necessary, therefore, we used two models – *in vitro* model of tumor cell-PBMC coculture and *in vivo* model of mouse xenografts. We chose the coculture study model as it involves the cultivation of different types of cells in the same conditions and allows the exploration of dynamic interactions between cancer-immune cells (Bogdanowicz and Lu 2014). Our model did not allow for direct cell-to-cell contact and was focused on paracrine signaling and response to soluble signaling factors.

FIGURE 2 | Changes in chemokine secretion pattern and expression of tumor cell markers upon CCR2 inhibition. Differences in secretion of CXCL8 (A), CCL2 (B) and VEGF (C) by ELISA when 143B cells were pretreated or not with 500 nM of CCR2 antagonist. The difference is shown as a sum of cytokine secretion levels from untreated (vehicle, red squares) to treated conditions (orange squares) in 143B or PBMC mono-culture and transwell under hypoxic or normoxic conditions. (D, E) Changes in CAIX, PD-L1, CD44, CCR2, and VEGFR surface expression on 143B cells by MFI (D) and by percentage of live cells (E) in the coculture when cells were pretreated or not with 500 nM of CCR2 antagonist under hypoxic or normoxic conditions, (F) CXCR1 surface expression by percentage on live 143B cells in mono-culture and coculture when cells were pretreated or not with 500 nM of CCR2 antagonist under hypoxic or normoxic conditions. (G) Multiple variables analysis for PD-L1, CCL2, CD44 and CAIX expression in hypoxia comparing transwell coculture phenotype with mono-culture when cells were treated CCR2 antagonist. (H) Multiple variables analysis for VEGFR, CD44, CCL2, CAIX expression in hypoxia comparing transwell coculture phenotype when cells are treated with vehicle versus CCR2 antagonist. (I) Changes in CD11b+ CD86+, CD11b+ CD163+, CD11b+ CD206+, CCR2+, CD11b+ CCR2+, and PD-L1+ percentage of CD45+ cells by flow cytometry on PBMCs in their coculture with 143B cells pretreated or not with CCR2 antagonist under hypoxic or normoxic conditions. * $p < 0.05$, ** $p < 0.01$, *** $p < 0.001$, significance was determined using the Student's *t*-test, $n = 3$ per experimental group.

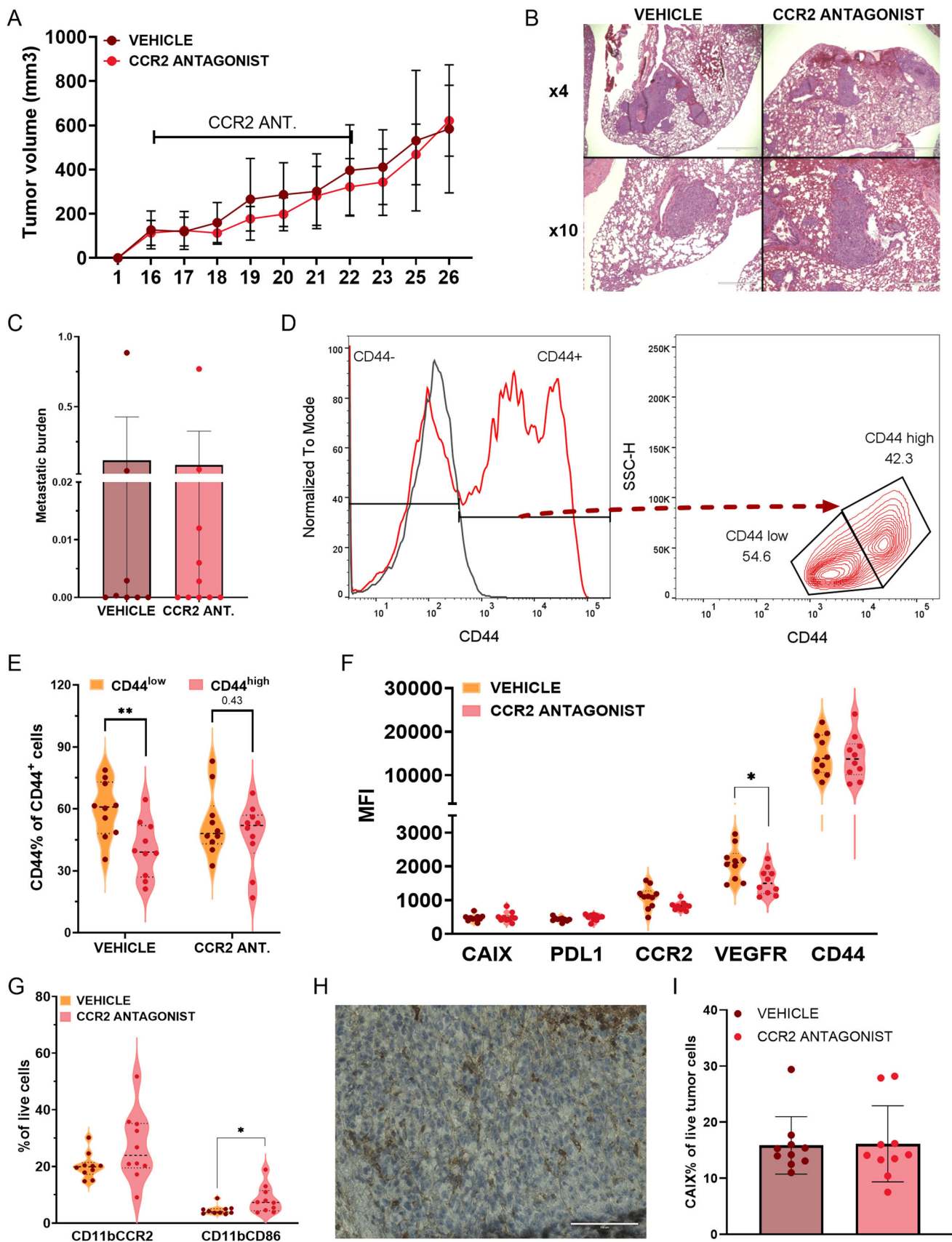


FIGURE 3 | Legend on next page.

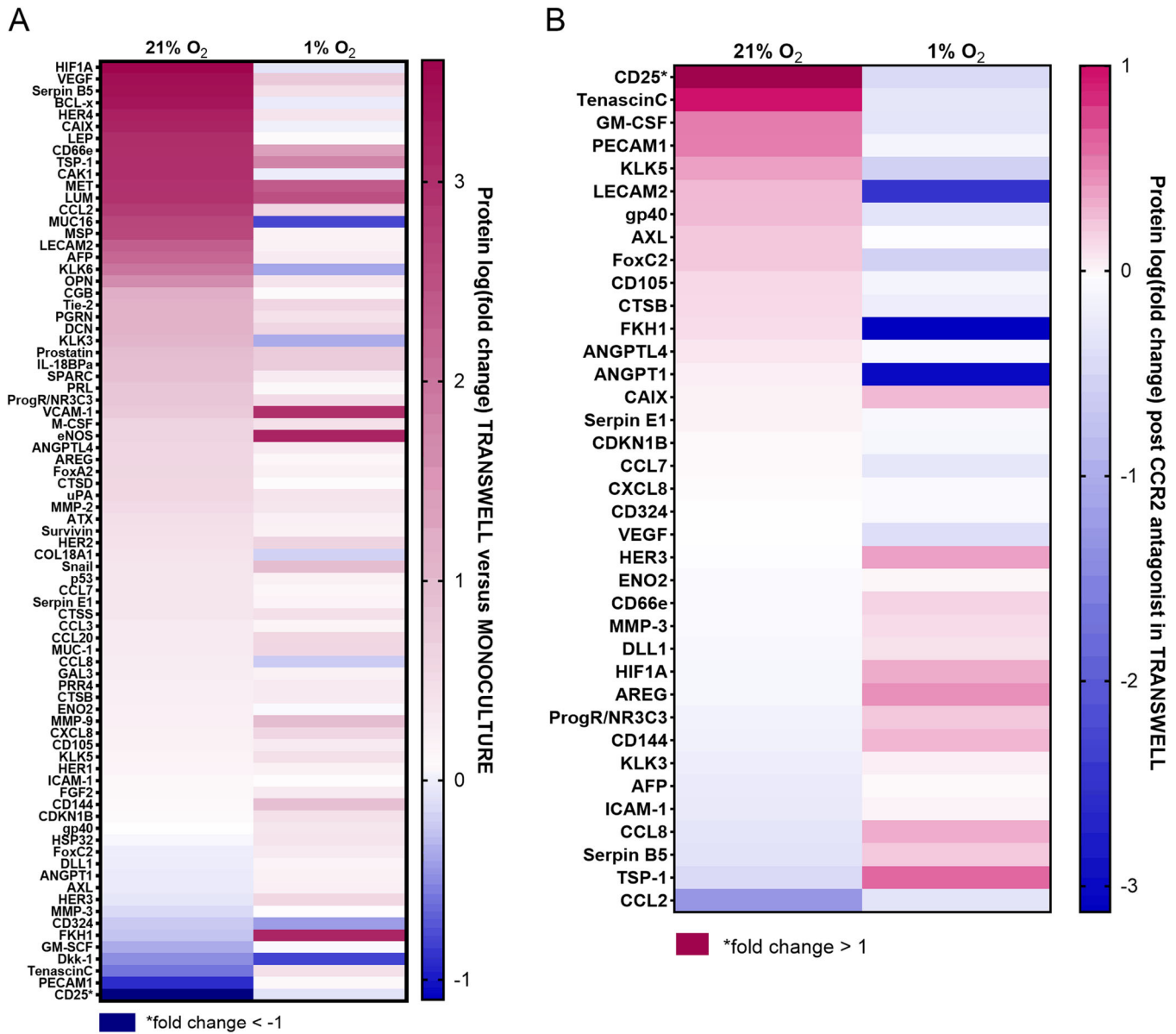


FIGURE 4 | Selected human cancer-related protein analysis on 143B cells comparing mono-culture to coculture and CCR2 antagonist response in 143B cells from coculture in hypoxia versus normoxia. (A) Protein array depicting differential protein expression fold changes of transwell compared to mono-culture in hypoxia and normoxia. (B) Protein array depicting different fold changes in protein expression of CCR2 treated versus vehicle control cells from coculture in hypoxia and normoxia.

FIGURE 3 | In vivo treatment with CCR2 antagonist did not affect tumor growth or metastasis, but altered surface receptor expression on tumor cells and infiltrating monocytes/macrophages. (A) 143B tumor growth dynamics in Nude mice when they were administered with CCR2 antagonist (red circles) versus vehicle controls (brown circles). Data shown as Means \pm SD, $n = 10$ per experimental group. (B, C) Metastatic tumor burden in lungs of CCR2 antagonist-treated mice (brown bar and circles) compared to vehicle control (red bar and circles), scale bars of IHC images: top ($\times 4$ magnification) – 400 μm , bottom ($\times 4$ magnification)–1000 μm . (D) Gating strategy of CD44 expression and quantification of the % of CD44^{low} and CD44^{high} in CD44⁺ cells. (E) Differences of CD44 expression on tumor cells: population having low expression of CD44 (CD44^{low}) and population having high expression of CD44 (CD44^{high}). (F) Dot and violin plots depicting MFI of CAIX, PD-L1, CCR2, VEGFR and CD44 surface protein staining on tumor cells from mice treated with vehicle control (pink with red circles) or CCR2 antagonist (yellow with brown circles). Each data point represents a separate tumor sample from mice. (G) CD11bCCR2 and CD11bCD86 surface expression differences in monocytes/macrophages from tumors of mice treated with CCR2 antagonist (yellow with brown circles) versus controls (pink with red circles). (H) CAIX expression on 143B tumors by IHC; scale bars–100 μm . (I) Percentage of CAIX+ cells in tumors from mice treated with vehicle versus CCR2 antagonist by flow cytometry. Each data point represents a separate tumor sample from mice, $n = 10$ per experimental group. * $p < 0.05$, ** $p < 0.01$, *** $p < 0.001$, significance was determined using the Student's t -test.

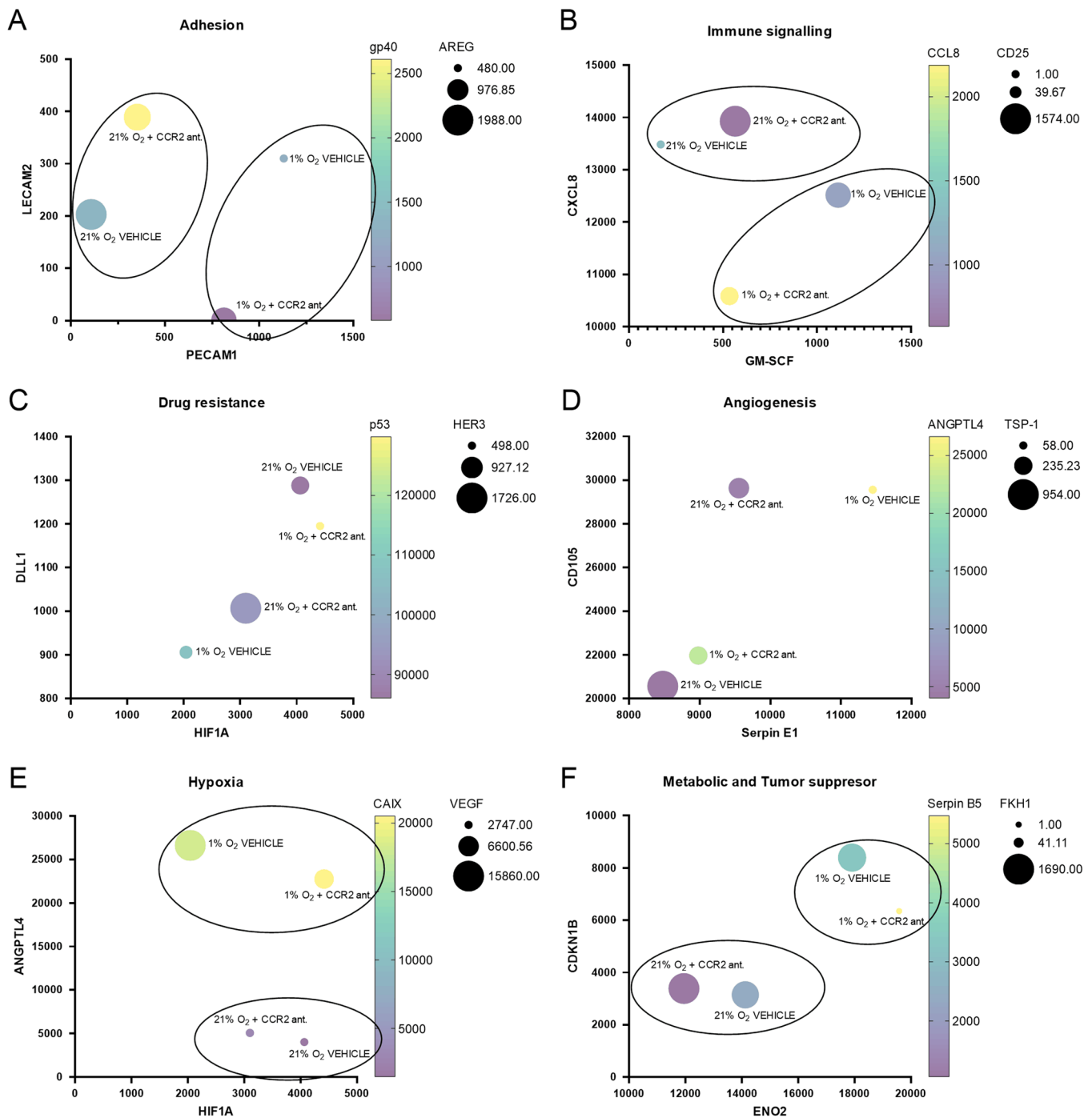


FIGURE 5 | Selected functional clusters of human cancer-related protein analysis of 143B cells comparing mono-culture to coculture and CCR2 antagonist response in 143B cells from coculture in hypoxia versus normoxia. Multiple variables analysis was performed with selected cancer-related target related to certain cell signaling pathway: (A) LECAM2, PECAM1, AREG and gp40–cell adhesion cluster. (B) CXCL8, GM-CSF, CCL8 and CD25–immune signaling cluster. (C) DLL1, HIF1A, p53 and HER3–drug resistance cluster. (D) Serpin E1, CD105, ANGPTL4 and TSO-1–angiogenesis cluster, (E) ANGPTL4, HIF1A, CAIX and VEGF – hypoxia cluster. (F) CDKN1B, ENO2, Serpin B5 and FKHI–metabolic and tumor suppressor cluster.

First, we interrogated the effect of the CCR2 antagonist on the ability of 143B cells to secrete chemokines CXCL8, CCL2, and VEGF. All these proangiogenic and pro-inflammatory cytokines are angiogenic and implicated in cancer metastasis (Gálvez et al. 2005; Pausch et al. 2020). Importantly, CXCL8 and VEGF were shown to be increased in the blood serum of patients with osteosarcoma (Jiang et al. 2017). Comparing cytokine secretion differences in the coculture model when 143B cells were

exposed to PBMC-secreted molecules to 143B mono-culture we observed an increase in CXCL8 secretion in the coculture. In mono-cultures, PBMCs secreted more CXCL8 than 143B cells, and this difference was more notable in normoxia than in hypoxia. Conversely, in transwell coculture there was a further increase in CXCL8 secretion in both oxygen conditions. Interestingly, the CCR2 antagonist was effective at decreasing CXCL8 secretion by PBMCs only in normoxia. Similarly to

CXCL8, CCL2 secretion was also more pronounced in PBMCs but not in 143B cells. Although CCL2 level increased in the transwell coculture under normoxia it decreased significantly in hypoxia. The mechanism of such downregulation of CCL2 secretion in hypoxia is unclear. Treatment with CCR2 antagonist dramatically increased CCL2 production across experimental conditions. We believe this is a compensatory effect to blockade of the CCR2 receptor by CCR2 antagonist preventing CCL2 binding.

The VEGF-VEGFR axis is implicated in tumor neo-angiogenesis and represents a prognostic marker in osteosarcoma patients (Zhang et al. 2021). Notably, the VEGF secretion pattern was different from that of CCL2 and CXCL8, as this cytokine was produced mainly by 143B cells and not PBMCs in monocultures. In the coculture, we noticed that increased VEGF secretion was more pronounced in hypoxia than in normoxia. In turn, the CCR2 antagonist was more effective in decreasing VEGF secretion in hypoxia, with increased VEGFR expression on 143B cells in the coculture. In summary, we demonstrated that CCR2 antagonist differentially affects CXCL8 secretion in normoxia and VEGF secretion in hypoxia.

Next, we examined changes in expression levels of PD-L1, CD44, CAIX, and CCR2 on the surface of 143B cells in the transwell coculture model. CD44, cell surface adhesion receptor and stem cell marker, regulates cancer progression and metastasis (Basakran 2015; Skandalis 2023). CD44 is a transmembrane glycoprotein, a receptor for hyaluronic acid, that plays a role in cell-to-cell interactions via osteopontin, collagens, and MMP. Interest in CD44 studies in osteosarcoma has gained speed, as it is associated with tumor progression and metastasis in preclinical osteosarcoma studies (Gvozdenovic et al. 2013) and is associated with worse survival in osteosarcoma patients (Gao et al. 2015). CD44 promotes osteosarcoma cell migration and proliferation and positively correlates with osteosarcoma immune checkpoint proteins such as PD-L1, a ligand for programmed cell death protein 1 (PD-1), which is a T-cell co-inhibitory receptor (Brahmer et al. 2012; Ji et al. 2023). In agreement with this notion, we observe that 143B cells have high expression of both markers, PD-L1 and CD44, and hypoxia causes downregulation of both, PD-L1 and CD44 expression. In contrast, in breast cancer studies hypoxia upregulated CD44 expression on tumor cells (Krishnamachary et al. 2012). In our study, the addition of CCR2 antagonist increased PD-L1 and CD44 expression in normoxia but failed to do so in hypoxia.

We also assessed changes of CAIX on 143B cells, a key enzyme for cancer cell survival in hypoxia (Pastorekova and Gillies 2019). This surface protein, helps cancer cells to survive in hypoxia by maintaining the physiological pH in cancer cells and acidifying the TME (Pastorekova and Gillies 2019). We observed a significant increase of CAIX expression on the surface of 143B cells in hypoxia, and even more so - in their coculture with PBMCs. CCR2 antagonist did decrease CAIX expression on 143B cells in hypoxia, although this change was not statistically significant. The possible mechanisms linking the CCL2-CCR2 axis and CAIX expression need to be further explored. In our study, CCR2 expression only slightly decreased on 143B cells in hypoxia. But contrary to that, there was a significant increase in CCR2 surface expression in

CD45⁺CD11b⁺ cells under hypoxia, showing that this cell subset might be more sensitive to hypoxia. Treatment with CCR2 antagonist increased CCR2 surface expression on 143B cells in transwell across different oxygen conditions and was likely a compensatory effect. Although previous studies have reported diminished CCR2 expression in M2 macrophages in hypoxia (Araya et al. 2019) we observed the opposite effect.

Lastly, we went on to explore the effects of CCR2 blockade on the same selected cellular markers in the in vivo model. Although targeting the CCL2-CCR2 axis in osteosarcoma remains an attractive immunotherapy option, a rich body of evidence today shows that CCR2 blockade as monotherapy does not work (Fei et al. 2021). In agreement with these observations, in our study treatment of mice with CCR2 antagonist in vivo did not slow tumor progression or stop metastasis compared to vehicle control - it is likely due to various oxygen tensions in the tumor-altering treatment response as we determined in the coculture model. Flow cytometry analysis of harvested osteosarcoma tumors from mice, treated with CCR2 antagonist showed alterations in tumor CD44, VEGFR, and PD-L1 expression as well as CD86 expression on monocytes/macrophages compared to vehicle controls. CCR2 blockade increased the fraction of VEGFR⁺, as well as PD-L1⁺ tumor cells, which might indicate an evasive mechanism when an alternative proangiogenic, immunosuppressive pathway is activated. CCR2 blockade also increased the fraction of CD44⁺ cells. Interestingly, we observed two populations having either low or high expression of CD44. CCR2 antagonist shifted the cells from CD44^{low} to CD44^{high} in this way increasing overall CD44 expression. In tumor stroma analysis we noted an increase in CD11b⁺CD86⁺ cells after CCR2 inhibition. CD86 is a costimulatory molecule that CD11b⁺ cells express as a response to pro-inflammatory signals (Orecchioni et al. 2019). Tumor-associated macrophages (TAMs) that express CD86⁺ can exert both pro-tumorigenic and anti-tumorigenic functions depending on their activation state (Cendrowicz et al. 2021). Therefore, an increase in the number of the subset of these cells could potentially be a desired effect of CCR2 blockade-related treatment.

CCR2 antagonist ineffectiveness in vivo could be related to a hypoxic microenvironment. CAIX expression is avid in these tumors and signifies an altered oxygen supply. Our in vitro data suggest differential surface protein expression as well as cytokine secretion in response to CCR2 antagonists in hypoxia as compared to normoxia. Therefore we performed a more in-depth proteome analysis of cancer-related targets in tumor cells grown in coculture with PBMC and when they are subjected to CCR2 antagonist in hypoxia versus normoxia. Proteome analysis revealed differential expression patterns in tumor cells. Hypoxia-related proteins such as CAIX and HIF1A are further increased with CCR2 antagonist administration in hypoxia. Importantly, VEGF was downregulated in hypoxic coculture when CCR2 antagonist was added, and we observed the same trend in mice tumors' VEGFR expression. Also, proteins associated with drug resistance, such as DLL1 and p53 were upregulated when hypoxic coculture was treated with CCR2 antagonist. These hypoxia-driven mechanisms are likely responsible for poor response to CCR2 treatment.

In summary, our findings show that hypoxic conditions alter the expression of different cellular markers and impair CCR2

antagonist effects in the experimental osteosarcoma model. CCR2 inhibition in the 143B cell model has differential effects on protein surface expression and cytokine secretion depending on oxygen levels. CCL2-CCR2 axis blockade with CCR2 antagonist does not slow 143B tumor growth or metastasis but alters TME by decreased VEGFR and shifts the CD44 expressing cell population towards CD44^{high}. A Proteome array of 143B cells from coculture with PBMCs reveals upregulation of various angiogenesis, hypoxia, cell adhesion, and drug resistance-related proteins that can explain poor treatment response in mice. Changes in CAIX and HIF1A, as well as DLL1 and p53 upregulation are of particular interest.

Our data show potential for dual targeting of the CCL2-CCR2 axis with HIF1A or CAIX inhibitors in the future. In addition, we reveal prospects for CCL2-CCR2 axis blockade with inhibitors targeting VEGFR or CD44 expression or activity. Lastly, we show the benefits of the tumor cell-PBMC coculture model as a tool to better delineate the tumor cell phenotypes compared to mono-cultures.

Author Contributions

A.P. designed the experiments, performed coculture, proteomics, and animal experiments, analyzed the data, and wrote the manuscript. Just.M. and A.S. performed animal-related experiments. Just.M. helped with proteomics work. D.P. helped with histology analysis. S.A. performed cell culture work. J.M., A.Ž., and D.M. were responsible for the final manuscript revision. A.L. contributed to experimental design, coculture experiments, data analysis, and manuscript preparation, and final revision. All of the authors reviewed the manuscript and approved its final version.

Acknowledgments

St. Baldrick's Foundation grant in part supported this study.

Conflicts of Interest

The authors declare no conflicts of interest.

Data Availability Statement

The data supporting this study's findings are available from the corresponding authors upon request.

References

Abou Khouzam, R., K. Brodaczevska, A. Filipiak, et al. 2020. "Tumor Hypoxia Regulates Immune Escape/Invasion: Influence on Angiogenesis and Potential Impact of Hypoxic Biomarkers on Cancer Therapies." *Frontiers in Immunology* 11: 613114. <https://doi.org/10.3389/fimmu.2020.613114>.

Araya, P., J. Romero, F. Delgado-López, et al. 2019. "HMGB1 Decreases CCR-2 Expression and Migration of M2 Macrophages Under Hypoxia." *Inflammation Research* 68, no. 8: 639–642. <https://doi.org/10.1007/s00011-019-01249-5>.

Basakran, N. S. 2015. "CD44 as a Potential Diagnostic Tumor Marker." *Saudi Medical Journal* 36, no. 3: 273–279. <https://doi.org/10.15537/smj.2015.3.9622>.

Bogdanowicz, D. R., and H. H. Lu. 2014. "Multifunction Co-Culture Model for Evaluating Cell-Cell Interactions." *Methods in Molecular Biology* 1202: 29–36. https://doi.org/10.1007/7651_2013_62.

Bosse, K. R., R. G. Majzner, C. L. Mackall, and J. M. Maris. 2020. "Immune-Based Approaches for the Treatment of Pediatric Malignancies." *Annual Review of Cancer Biology* 4: 353–370.

Brahmer, J. R., S. S. Tykodi, L. Q. M. Chow, et al. 2012. "Safety and Activity of Anti-PD-L1 Antibody in Patients With Advanced Cancer." *New England Journal of Medicine* 366, no. 26: 2455–2465. <https://doi.org/10.1056/NEJMoa1200694>.

Campanile, C., M. J. E. Arlt, S. D. Krämer, et al. 2013. "Characterization of Different Osteosarcoma Phenotypes by PET Imaging in Preclinical Animal Models." *Journal of Nuclear Medicine* 54, no. 8: 1362–1368. <https://doi.org/10.2967/jnumed.112.115527>.

Cendrowicz, E., Z. Sas, E. Bremer, and T. P. Rygiel. 2021. "The Role of Macrophages in Cancer Development and Therapy." *Cancers* 13, no. 8: 1946. <https://doi.org/10.3390/cancers13081946>.

Chen, Q., W. Sun, Y. Liao, et al. 2015. "Monocyte Chemotactic Protein-1 Promotes the Proliferation and Invasion of Osteosarcoma Cells and Upregulates the Expression of AKT." *Molecular Medicine Reports* 12, no. 1: 219–225. <https://doi.org/10.3892/mmr.2015.3375>.

Dou, B., T. Chen, Q. Chu, G. Zhang, and Z. Meng. 2021. "The Roles of Metastasis-Related Proteins in the Development of Giant Cell Tumor of Bone, Osteosarcoma and Ewing's Sarcoma." *Technology and Health Care* 29, no. S1: 91–101. <https://doi.org/10.3233/THC-218010>.

Fei, L., X. Ren, H. Yu, and Y. Zhan. 2021. "Targeting the CCL2/CCR2 Axis in Cancer Immunotherapy: One Stone, Three Birds?" *Frontiers in Immunology* 12: 771210. <https://doi.org/10.3389/fimmu.2021.771210>.

Gálvez, B. G., L. Genis, S. Matías-Román, et al. 2005. "Membrane Type 1-Matrix Metalloproteinase Is Regulated by Chemokines Monocyte-Chemoattractant Protein-1/ccl2 and Interleukin-8/CXCL8 in Endothelial Cells During Angiogenesis." *Journal of Biological Chemistry* 280, no. 2: 1292–1298. <https://doi.org/10.1074/jbc.M408673200>.

Gao, Y., Y. Feng, J. K. Shen, et al. 2015. "CD44 Is a Direct Target of miR-199a-3p and Contributes to Aggressive Progression in Osteosarcoma." *Scientific Reports* 5: 11365. <https://doi.org/10.1038/srep11365>.

Gvozdenovic, A., M. J. Arlt, C. Campanile, et al. 2013. "CD44 Enhances Tumor Formation and Lung Metastasis in Experimental Osteosarcoma and Is an Additional Predictor for Poor Patient Outcome." *Journal of Bone and Mineral Research* 28, no. 4: 838–847. <https://doi.org/10.1002/jbmr.1817>.

Ji, H., L. Kong, Y. Wang, et al. 2023. "CD44 Expression Is Correlated With Osteosarcoma Cell Progression and Immune Infiltration and Affects the Wnt/ β -catenin Signaling Pathway." *Journal of Bone Oncology* 41: 100487. <https://doi.org/10.1016/j.jbo.2023.100487>.

Jiang, H., X. Wang, W. Miao, B. Wang, and Y. Qiu. 2017. "CXCL8 Promotes the Invasion of Human Osteosarcoma Cells by Regulation of PI3K/Akt Signaling Pathway." *APMIS* 125, no. 9: 773–780. <https://doi.org/10.1111/apm.12721>.

Krishnamachary, B., M. F. Penet, S. Nimmagadda, et al. 2012. "Hypoxia Regulates CD44 and Its Variant Isoforms Through HIF-1 α in Triple Negative Breast Cancer." *PLoS One* 7, no. 8: e44078. <https://doi.org/10.1371/journal.pone.0044078>.

Liu, J. F., P. C. Chen, T. M. Chang, and C. H. Hou. 2020. "Monocyte Chemoattractant Protein-1 Promotes Cancer Cell Migration via c-Raf/MAPK/AP-1 Pathway and MMP-9 Production in Osteosarcoma." *Journal of Experimental & Clinical Cancer Research* 39, no. 1: 254. <https://doi.org/10.1186/s13046-020-01756-y>.

von Luetichau, I., S. Segerer, A. Wechselberger, et al. 2008. "A Complex Pattern of Chemokine Receptor Expression Is Seen in Osteosarcoma." *BMC Cancer* 8: 23. <https://doi.org/10.1186/1471-2407-8-23>.

Mayr, L., C. Pirker, D. Löttsch, et al. 2017. "CD44 Drives Aggressiveness and Chemoresistance of a Metastatic Human Osteosarcoma Xenograft Model." *Oncotarget* 8: 114095–114108. <https://doi.org/10.18632/oncotarget.23125>.

McDonald, P. C., S. C. Chafe, and S. Dedhar. 2016. "Overcoming Hypoxia-Mediated Tumor Progression: Combinatorial Approaches Targeting pH Regulation, Angiogenesis and Immune Dysfunction."

Frontiers in Cell and Developmental Biology 4: 27. <https://doi.org/10.3389/fcell.2016.00027>.

McDonald, P. C., and S. Dedhar. 2014. "Carbonic Anhydrase IX (CAIX) as a Mediator of Hypoxia-Induced Stress Response in Cancer Cells." *Sub-Cellular Biochemistry* 75: 255–269.

Meltzer, P. S., and L. J. Helman. 2021. "New Horizons in the Treatment of Osteosarcoma." *New England Journal of Medicine* 385, no. 22: 2066–2076. <https://doi.org/10.1056/NEJMra2103423>.

Mirzadegan, T., F. Diehl, B. Ebi, et al. 2000. "Identification of the Binding Site for a Novel Class of CCR2b Chemokine Receptor Antagonists." *Journal of Biological Chemistry* 275, no. 33: 25562–25571. <https://doi.org/10.1074/jbc.M000692200>.

Oda, S., Y. Uchida, M. D. Aleo, et al. 2021. "An In Vitro Coculture System of Human Peripheral Blood Mononuclear Cells With Hepatocellular Carcinoma-Derived Cells for Predicting Drug-Induced Liver Injury." *Archives of Toxicology* 95, no. 1: 149–168. <https://doi.org/10.1007/s00204-020-02882-4>.

Orecchioni, M., Y. Ghosheh, A. B. Pramod, and K. Ley. 2019. "Macrophage Polarization: Different Gene Signatures in M1(LPS+) vs. Classically and M2(LPS-) vs. Alternatively Activated Macrophages." *Frontiers in Immunology* 10: 1084. <https://doi.org/10.3389/fimmu.2019.01084>.

Pastorekova, S., and R. J. Gillies. 2019. "The Role of Carbonic Anhydrase IX in Cancer Development: Links to Hypoxia, Acidosis, and Beyond." *Cancer and Metastasis Reviews* 38, no. 1-2: 65–77. <https://doi.org/10.1007/s10555-019-09799-0>.

Pausch, T. M., E. Aue, N. M. Wirsik, et al. 2020. "Metastasis-Associated Fibroblasts Promote Angiogenesis in Metastasized Pancreatic Cancer via the CXCL8 and the CCL2 Axes." *Scientific Reports* 10: 5420. <https://doi.org/10.1038/s41598-020-62416-x>.

Rasouli, M., and F. Safari. 2024. "Principles of Indirect Co-Culture Method Using Transwell." *Methods in Molecular Biology*: 1–7. https://doi.org/10.1007/978-1-093-03537-1_537.

Sceneay, J., M. T. Chow, A. Chen, et al. 2012. "Primary Tumor Hypoxia Recruits CD11b+/Ly6Cmed/Ly6G+ Immune Suppressor Cells and Compromises NK Cell Cytotoxicity in the Premetastatic Niche." *Cancer Research* 72, no. 16: 3906–3911. <https://doi.org/10.1158/0008-5472.CAN-11-3873>.

Skandalis, S. S. 2023. "CD44 Intracellular Domain: A Long Tale of a Short Tail." *Cancers* 15, no. 20: 5041. <https://doi.org/10.3390/cancers15205041>.

Thakur, M. D., C. J. Franz, L. Brennan, et al. 2022. "Immune Contexture of Paediatric Cancers." *European Journal of Cancer* 170: 179–193. <https://doi.org/10.1016/j.ejca.2022.03.012>.

Tu, M. M., H. A. Abdel-Hafiz, R. T. Jones, et al. 2020. "Inhibition of the CCL2 Receptor, CCR2, Enhances Tumor Response to Immune Checkpoint Therapy." *Communications Biology* 3, no. 1: 720. <https://doi.org/10.1038/s42003-020-01441-y>.

Uluçkan, Ö., A. Segaliny, S. Botter, J. M. Santiago, and A. J. Mutsaers. 2015. "Preclinical Mouse Models of Osteosarcoma." *BoneKEY Reports* 4: 670. <https://doi.org/10.1038/bonekey.2015.37>.

Vakkila, J., R. Jaffe, M. Michelow, and M. T. Lotze. 2006. "Pediatric Cancers Are Infiltrated Predominantly by Macrophages and Contain a Paucity of Dendritic Cells: A Major Nosologic Difference With Adult Tumors." *Clinical Cancer Research* 12, no. 7 Pt 1: 2049–2054. <https://doi.org/10.1158/1078-0432.CCR-05-1824>.

Arifin, W. N., and W. M. Z. Wan Mohammad. 2017. "Sample Size Calculation in Animal Studies Using Resource Equation Approach." *Malaysian Journal of Medical Sciences* 24, no. 5: 101–105. <https://doi.org/10.21315/mjms2017.24.5.11>.

Xu, M., Y. Wang, R. Xia, Y. Wei, and X. Wei. 2021. "Role of the CCL2-CCR2 Signalling Axis in Cancer: Mechanisms and Therapeutic Targeting." *Cell Proliferation* 54, no. 10: e13115. <https://doi.org/10.1111/cpr.13115>.

Yoshimura, T. 2018. "The Chemokine MCP-1 (CCL2) in the Host Interaction With Cancer: A Foe or Ally?" *Cellular & Molecular Immunology* 15, no. 4: 335–345. <https://doi.org/10.1038/cmi.2017.135>.

Zhang, C., L. Wang, C. Xiong, R. Zhao, H. Liang, and X. Luo. 2021. "The Role of Vascular Endothelial Growth Factor as a Prognostic and Clinicopathological Marker in Osteosarcoma: A Systematic Review and Meta-Analysis." *Journal of Orthopaedic Surgery and Research* 16, no. 1: 738. <https://doi.org/10.1186/s13018-021-02888-3>.

Supporting Information

Additional supporting information can be found online in the Supporting Information section.